JOURNAL OF THE PHYSICAL SOCIETY OF JAPAN, Vol. 42, No. 1, JANUARY, 1977

Electronic and Ionic Conduction in $Cu_{2-\delta}Se$, $Cu_{2-\delta}S$ and $Cu_{2-\delta}(Se, S)$

Tomonori ISHIKAWA and Shin-ya MIYATANI

Department of Physics, Faculty of Science, Kanazawa University, Kanazawa

(Received May 24, 1976)

Using the galvanic cell $Cu|CuBr \cdot C_6H_{12}N_4CH_3Br|Cu_{2-\delta}VI|Pt$, the deviation δ from the stoichiometric composition is varied up to 0.2 for $Cu_{2-\delta}Se$, $Cu_{2-\delta}S$ and their alloys. Electronic conductivity, thermoelectric power and Hall coefficient are measured as functions of e.m.f. of the cell, E, and of temperature, T, (20°C~200°C). The phase diagrams are constructed from these results, especially from E vs T plots, and the electrical properties are interpreted by the use of a simple model. Further, the ionic conductivity is measured with the use of the cell in low temperature phase as well as in high temperature one. The value of E seems not to represent the Fermi kinetic energy even in the high temperature phase having the average structure. This is because of the largeness of δ, and can be interpreted as being due to the screening effect of carriers (holes) on copper ion vacancies.

§1. Introduction

The crystallographic structures,[1] the phase diagrams[2-7] and the electrical properties[8-12] of the compounds $Cu_{2-\delta}VI$ have been studied by several investigators. The high temperature phases of these compounds are characterized by the stability in a very wide range of non-stoichiometricity, δ, and large ionic conduction together with the hole conduction coming from the deficiency of copper. These characteristics are attributed to the special crystallographic structure, the so-called "average structure" where copper ions are distributed statistically over a number of available sites.[1]

For the study of these compounds, the use of the galvanic cell $Cu|Cu^+$ ion conductor|Specimen|Pt is very helpful.[13] By sending a current across this cell, the value of δ can be varied continuously and further the e.m.f. of the cell, E, gives us the information of the chemical potential of Cu atom in the specimen. As Cu^+ ion conductor, CuI or CuBr is available at higher temperatures.[14] Recently a purely ionic conductor available at lower temperatures (<200°C) was found by T. Takahashi, O. Yamamoto and S. Ikeda.[15] This permits us to study these compounds in detail below 200°C. The purpose of the present work is to show the usefulness of this new ionic conductor and to present new data for the study of the mixed conductors like the present compounds.

Here we give a short review of the typical experimental method with the use of the cell $Cu|Cu^+$ ion conductor|Specimen|Pt.[16] Figure 1(a) shows a schematic diagram of the arrangement for the conductivity measurement, where P(Pt), S(specimen), I(ionic conductor) and C(Cu) form a galvanic cell. By sending a current across C and P, we can vary the Cu amount in the specimen and know the value of its change by Faraday's Law (coulometric titration). The electronic conductivity σ_e of the specimen may be found by measuring the potential drop between two metallic probes, p_1 and p_2, while

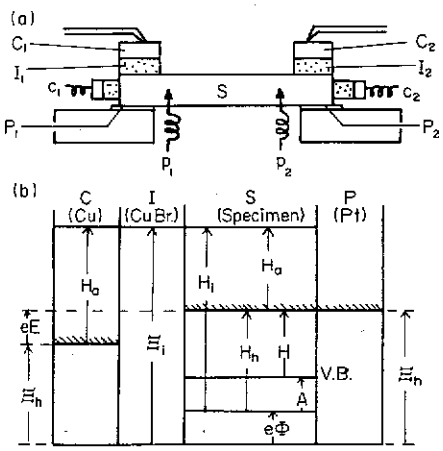

Fig. 1. (a) Schematic diagram of the arrangement used for measuring the conductivity. 'I' stands for $CuBr \cdot C_6H_{12}N_4CH_3Br$. (b) Schematic energy diagram of the galvanic cell Pt|Specimen|I|Cu.

sending a current through metallic electrodes, P_1 and P_2, and the ionic conductivity σ_i may be found by measuring the potential drop between two ionic probes, c_1 and c_2, while sending a current through ionic electrodes, C_1 and C_2. In these procedures it is necessary to wait enough time for the stationary concentration gradient to build up (steady state method). From the time constant with which the concentration gradient is built up, we can also find the ionic conductivity (dynamic method). The e.m.f. of the cell, that is, the potential difference between P and C, increases as Cu in the specimen is removed.

We measure the various properties of the specimen as functions of E, keeping the temperature fixed. The e.m.f. E is related to the chemical potential of a Cu atom, H_a, by

$$eE = H_a(\mathrm{C}) - H_a(\mathrm{S}) \qquad (1)$$

where C and S in the parentheses refer to Cu electrode and specimen respectively. This relation is illustrated in Fig. 1(b), which is a schematic energy diagram of the cell. In Fig. 1(b) H is the chemical potential, the Σ electrochemical potential and Φ the electrostatic potential, and suffices i and h refer to Cu ion and hole respectively. As Cu in the specimen is removed, H_a decreases, resulting in the increase of E. In the case of average structure, H_i is insensitive to δ and hence Φ is also insensitive to δ.[17] Then the change of eE gives us the direct information of the change of H_h. If the position of the valence band edge (V.B. in Fig. 1) is not changed when δ is varied, then eE gives the Fermi kinetic energy H (the height of the Fermi level measured from the band edge) apart from an additive constant, say, A. If this simple relation holds, the measured various quantities plotted against eE can be compared with theoretical formulae expressed as functions of Fermi kinetic energy, making the analysis of the data very easy and clear. This is a typical method which we have always used in the previous works on silver chalcogenides. For the present compounds, however, the situation is somewhat more complicated and some modification is necessary as will be shown later.

§2. Experimental Results and Interpretation

The sample is prepared by melting the component materials in an evacuated silica tube. It is polycrystalline. Specimens are cut and ground to proper size as small as *e.g.* $5\times2\times0.5$ mm or smaller, in order to make the time required for titration or polarization as short as possible. For convenience, we call the high temperature phase as α and low one as β, that is, α(cubic) and β(tetragonal) for $Cu_{2-\delta}Se$ and α'(hexagonal), α(cubic) and β(orthorhombic) for $Cu_{2-\delta}S$.

2.1 E and σ_e vs T and phase diagram

(a) $Cu_{2-\delta}Se$

In Figs. 2 and 3 the electromotive force E of the galvanic cell $Cu|CuBr\cdot C_6H_{12}N_4CH_3Br|Cu_{2-\delta}Se|Pt$ and the electronic conductivity σ_e of $Cu_{2-\delta}Se$ are plotted against temperature T for various value of δ, which are indicated in Fig. 4(a) by the same roman letters a, b, . . . , l as in Figs. 2 and 3. It is seen in Fig. 2 that E in the α phase decreases with decreasing temperature, but at a certain temperature it begins to increase along a single curve AB except "f" ($\delta=0.015$) for which the E-T curve begins to deviate from the curve AB at a certain temperature. The curve AB represents the boundary between α and mixed phases in the phase

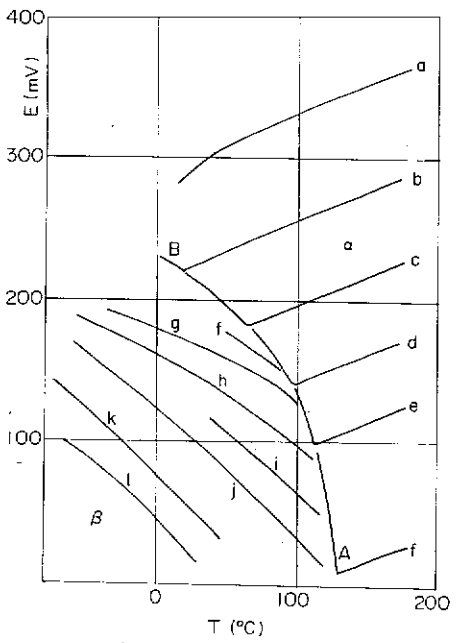

Fig. 2. E.m.f. E of the galvanic cell $Cu|CuBr\cdot C_6H_{12}N_4CH_3Br|Cu_{2-\delta}Se|Pt$ vs temperature T for $Cu_{2-\delta}Se$, whose δ-values are indicated in Fig. 4(a) by the same roman letters a, b, . . . , l as in this figure.

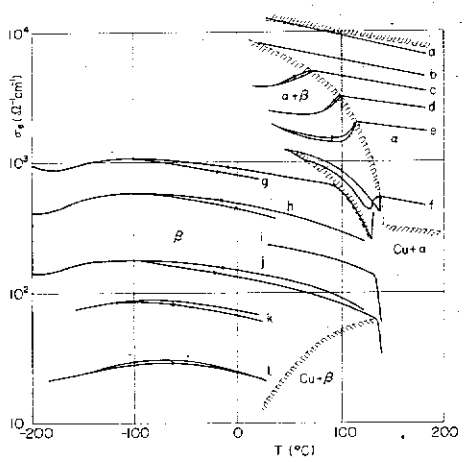

Fig. 3. Electronic conductivity σ_e vs T for $Cu_{2-\delta}Se$ with various δ-values. The roman letters a, b, . . . , l correspond to the same ones in Figs. 2 and 4.

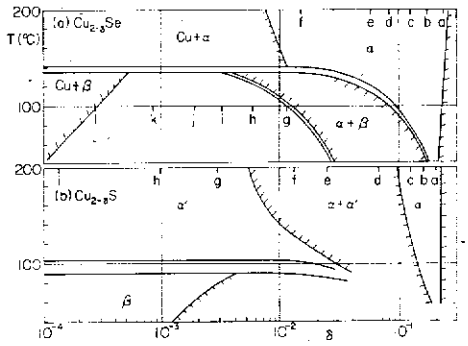

Fig. 4. Phase diagrams constructed from E vs T plots; (a) for $Cu_{2-\delta}Se$ and (b) for $Cu_{2-\delta}S$.

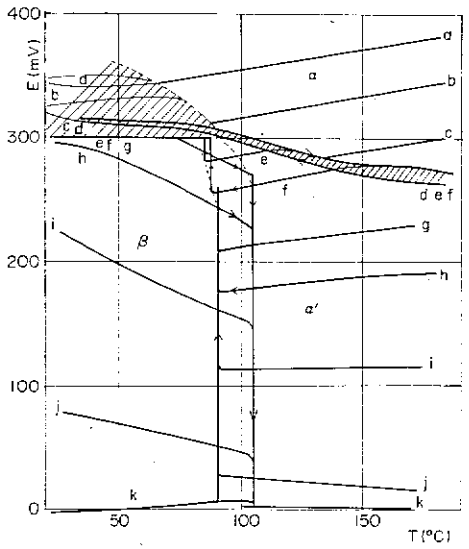

Fig. 5. E vs T for $Cu_{2-\delta}S$ with various δ-values as indicated in Fig. 4(b).

diagram. When we lower the temperature from α phase, we get, in general, the mixed phase of α and β. In order to get the single phase of β, we must supply Cu to the specimen of such a mixed phase. The curves "g ~ l" in Fig. 2 correspond to the compositions obtained by such supplying. Their temperature dependence is opposite to that of α phase. This is attributed to the difference of the entropies of a copper atom in the specimen when it is in α and β phases, since $\partial(eE)/\partial T$ is the entropy of a Cu atom in the specimen relative to that in metallic copper, i.e. $\partial(eE)/\partial T = S(Cu_2Se) - S(Cu)$. The difference of the entropies between α and β is estimated as about 14 k, k being the Boltzmann constant. (According to P. Kubaschewski and J. Nölting,[5] the latent heat at the $\beta \rightarrow \alpha$ transition is 6830 J/mol, leading the increase of entropy as 17.2 k/molecule.) As the temperature is raised in β phase, E decreases and joins to the curves AB or to the $E=0$ line. The curve AB represents again the boundary between β and mixed phase, and the $E=0$ line does the Cu-saturation limit. Thus we can construct the phase diagram as shown in Fig. 4(a). Besides, Fig. 3 shows another phase transition near -100 °C, which is consistent with the phase diagram already reported.[6,8]

(*b*) $Cu_{2-\delta}S$

The similar plots can be made for $Cu_{2-\delta}S$. In this case the situation is somewhat more complicated because of the existence of the two high temperature forms α(cubic) and α'(hexagonal). Figure 5 shows E vs T for $Cu_{2-\delta}S$ with various values of δ which are indicated in Fig. 4(b) by the same roman letters as in Fig. 5. Figure 6 is the corresponding σ_e vs T plots. Similarly to the case of $Cu_{2-\delta}Se$, the phase diagram can be constructed and is shown in Fig. 4(b) which is consistent with the phase diagram by E. H. Roseboom.[2] It is noticiable that the stable region of δ becomes very large near the transition temperature, *e.g.* $0 < \delta < 0.03$ at 100 °C. The existence of the djurleite phase could not be ascertained by the E-T plots.

(*c*) $Cu_{2-\delta}Se_ySe_{1-y}$

As noted above, $Cu_{2-\delta}Se$ has only one high temperature form α while $Cu_{2-\delta}S$ has two, α and α', in the range of $\delta < 0.2$. If a fraction of Se in $Cu_{2-\delta}Se$ is replaced by S, the α' form will appear at some Se/S ratio. This is in fact the case, as proved by X-ray analysis.[7] Figure 7

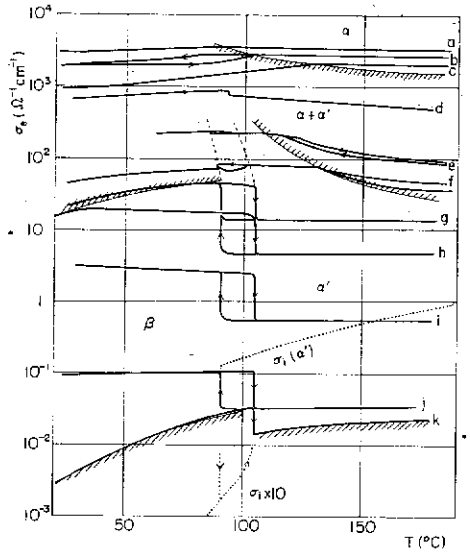

Fig. 6. σ_e vs T for $Cu_{2-\delta}S$ corresponding to Fig. 5.

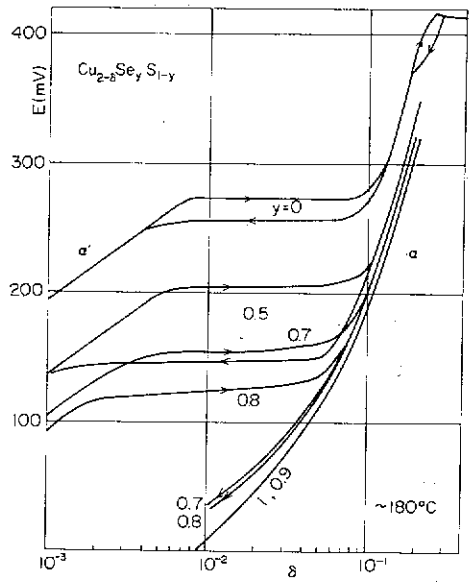

Fig. 7. The titration curves for $Cu_{2-\delta}Se_ySi_{1-y}$.

shows E vs δ in the coulometric titration at 175°C. When Cu is removed from the specimen (with $y<0.9$) at the α' phase, E increases along the classical line. At a certain E, E stops to increase even if the subtraction of Cu is continued. This corresponds to the coexistance of α' and α. When the whole specimen transforms to α, E begins to increase again. Conversely, if Cu is supplied to the specimen of the α, the hexagonal phase is recovered with some hysteresis for $y \lesssim 0.5$.

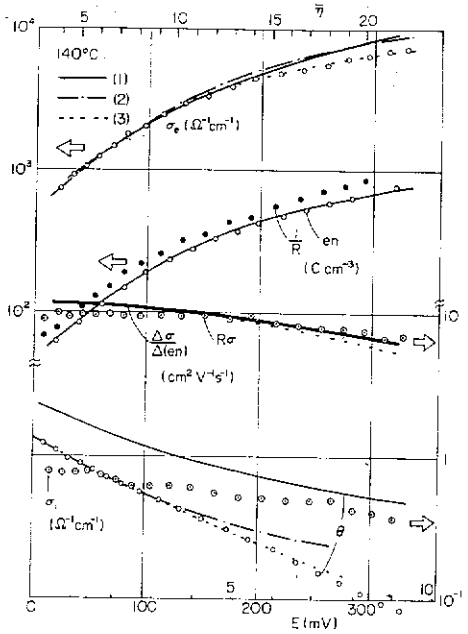

Fig. 8. σ_e, $1/R$, en, $R\sigma_e$, θ and σ_i vs E (lower abscissa) or $\bar{\eta}$ (upper abscissa) for α-$Cu_{2-\delta}Se$ at 140°C, R being the Hall coefficient, n the number density of holes, θ the thermoelectric power in the unit of k/e and σ_i the ionic conductivity. Three theoretical curves are also drawn.

2.2 *Electrical properties*

(*a*) α-$Cu_{2-\delta}Se$

Figure 8 shows the electronic conductivity σ_e, the concentration of deficient Cu multiplied by e, en, which is estimated from the titration amount, the inverse of Hall coefficient, $1/R$, the Hall mobility, $R\sigma_e$, the reduced thermoelectric power, θ, which is reduced to non-dimensional by the multiplication factor e/k, and the ionic conductivity, σ_i, at 140°C. They are all plotted against E. We note, at first, $R\sigma_e$ is nearly constant and, roughly speaking, equal to $\partial\sigma_e/\partial en$ which is shown by thick line in the figure. This means that, at titration, the number of removed Cu is equal to that of hole produced. In other words, the Cu-deficits are fully ionized. Thus, denoting the concentration of Cu-deficit and of hole as n_d and n_h respectively, we have $n_d=n_h\equiv n$. From the titration alone, we know only the value of en relative to the reference state (*e.g.* the state at $E=0$). But, using the above equality, we can estimate the absolute value of en by adding $\sigma_e/(\partial\sigma_e/\partial en)$ to the reference state. The values of en as shown by small circles in the figure are those estimated in this way. The equality $n_d=n_h$ is also seen by the

parallelism of en and $1/R$. Since the measured Hall voltages are so small that we cannot say anything about whether the difference between en and $1/R$ is attributed to some systematic errors or not.

In order to account for these experimental plots, let us assume that E represents the Fermi kinetic energy as mentioned in the preceding paragraph, that is, $H=eE+H_0$ (or, divided by kT, $\eta=\varepsilon+\eta_0$) where suffix 0 refers to the Cu-saturated state in which $E=0$. We assume further that the effective mass m^* and the relaxation time of scattering, τ, of holes are independent of its energy (model (1)). The theoretical formulae are then

$$en=e(m^*/m)^{\frac{3}{2}}N^{\frac{3}{2}}F_{\frac{1}{2}}(\eta);\quad N=(2kTm)^{\frac{3}{2}}/(3\pi^2\hbar^3), \tag{2}$$

$$\sigma_e=en\mu;\quad \mu=e\tau/m^*, \tag{3}$$

$$\theta=\frac{5}{3}\frac{F_{\frac{3}{2}}(\eta)}{F_{\frac{1}{2}}(\eta)}-\eta, \tag{4}$$

$$R\sigma_e=\mu, \tag{5}$$

where $F_r(\eta)$ is the Fermi-Dirac integral of order r. The thin curves in Fig. 8 are theoretical ones obtained by adjusting m^* and η_0 to get the best fit. It is seen that en is almost completely accounted for with $m^*=2.9$ m, and that σ_e and $R\sigma_e$ may be also accounted for if we neglect the difference between en and $1/R$ as experimental error and assume the mobility slightly decreasing with increasing en. However, the discrepancy for θ is so large that this model should be given up.

As an alternative one, we assume that the effective mass is constant but E does not represent the Fermi kinetic energy (model (2)). The $\ln(en)$ vs θ plot is accounted for by the theoretical one given by eqs. (2) and (4), at least in the small-E range. ($E<100$ mV), yielding the effective mass m^* to be $1.32\,m$ instead of $2.9\,m$. With this value of m^*, we have estimated η-values corresponding to en-values by the use of eq. (2) and have shown on the upper abscissa of Fig. 8. (We denote m^* and η defined in this way by $\bar{m}^*$ and $\bar{\eta}$, respectively. On the other hand, we denote by $\tilde{m}^*$ the m^* defined by using the relation $\eta=\varepsilon+\eta_0$.) The theoretical value of θ given by eq. (4) is shown by the chain line in Fig. 8, with which the experimental θ-values agree for the small-E range. To get better fit, we note that the mobility $R\sigma_e$ is not constant but slightly decreases with increasing en. Considering the fairly high degeneracy of holes, we have

$$\frac{\partial\sigma_e}{\partial(en)}=\mu(\eta)+\left(\frac{\partial\ln(en)}{\partial\eta}\right)^{-1}\frac{\partial\mu}{\partial\eta},\quad R\sigma_e=\mu(\eta), \tag{6}$$

$$\theta=\frac{\pi^2}{3}\frac{\partial\ln\sigma_e}{\partial\eta}=\theta_0+\frac{\pi^2}{3}\frac{1}{\mu}\frac{\partial\mu}{\partial\eta}, \tag{7}$$

where θ_0 is θ in the case of constant mobility. With this modification, we have a fairely good fit as shown by the dotted curves (3) in Fig. 8. The mean free path length is estimated to be $16\sim35$ Å which is fairly large in comparison with the atomic distance, showing that the Boltzmann equation is applicable.

Finally we note that the ionic conductivity σ_i decreases with increasing en. In the materials of the average structure like the present ones, we expect that the whole copper ions contribute to the ionic conduction. The mean mobility defined by $\bar{\mu}_i=\sigma_i/en_i$, n_i being the total Cu^+ density, is not constant but slightly decreases with increasing ε as given by $\bar{\mu}_i=1.2\times10^{-4}(1-0.041\varepsilon)\ \mathrm{cm^2V^{-1}s^{-1}}$. Further, the decrease of σ_i is not linear to δ and so can not be accounted for by the model that a certain number of copper ions is immobile. The reason of this decrease is not clear but it might be ascribed to electron-ion (hole-vacancy in our case) interaction.

(*b*) β-$Cu_{2-\delta}Se$

Figure 9 shows σ_e, en, θ, $R\sigma_e$ and $\Delta\sigma_e/\Delta(en)$,

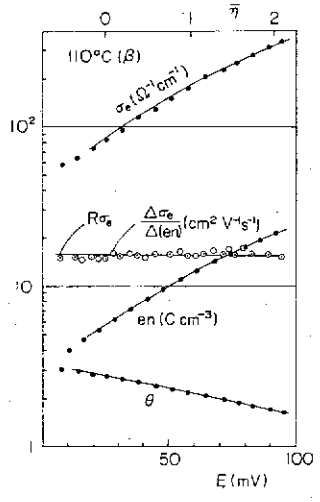

Fig. 9. σ_e, $R\sigma_e$, $\Delta\sigma_e/\Delta(en)$, en and θ vs E for β-$Cu_{2-\delta}Se$ at 110°C.

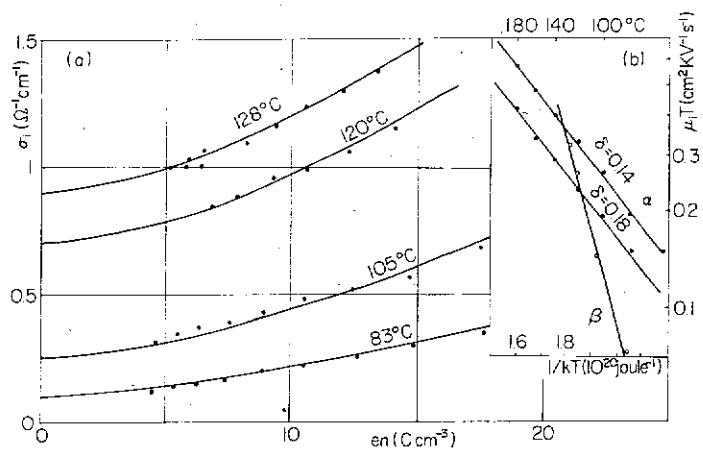

Fig. 10. (a) σ_i vs en and (b) $\mu_i T$ vs $1/kT$ for β-$Cu_{2-\delta}Se$, μ_i being the mobility of Cu^+ ions.

all plotted against E at 110°C, where $\Delta\sigma_e/\Delta(en)$ is the change of σ_e divided by the change of en at titration. As seen in the figure the equality, $R\sigma_e=\Delta\sigma_e/\Delta(en)$, is fairly well established. These experimental data can be consistently interpreted, as done for the α-phase, in terms of constant hole mass m^* and energy independent hole mobility μ and with the assumption that the number of stoichiometrically deficient copper atom is just equal to the number of holes, $n_d=n_h(\equiv n)$. We find $m^*=1.18\,m$ and the mean free path length is estimated to be $10\sim15$ Å, being again larger than the atomic distance.

In Fig. 10(a) the ionic conductivity σ_i is plotted against en, showing increasing σ_i with increasing en in contrast to the case of α-phase. This suggests that the lattice defects in β-phase are of Frenkel type. With the mass action law and $n_d=n_v-n_{in}$, where n_{in} and n_v are the concentration of interstitial ions and of vacancies respectively, and assuming that the mobilities of an interstitial ion and of a vacancy are equal to each other and equal to μ_i, we find for σ_i

$$\sigma_i=e\mu_i\sqrt{n_h^2+4f};\ f\equiv N_{in}N_0\exp(-w/kT), \quad (8)$$

where N_{in} and N_0 are the number densities of interstitial and normal sites, respectively, and w is the activation energy for generation of one pair of defects. The full curves in Fig. 10(a) show σ_i at several temperatures calculated according to eq. (8) with $w=0.23$ eV. Further, the temperature dependence of μ_i may be expressed by

$$\mu_i T=A\exp(-\Delta g/kT), \quad (9)$$

where Δg is the activation energy for ion jump. In Fig. 10(b) $\mu_i T$ is plotted against $1/kT$, yielding $\Delta g=0.41$ eV. For comparison, $\mu_i T$ in α-phase is also plotted for two specimens with fairly large δ-values, yielding $\Delta g=0.14$ eV.

(c) α'-$Cu_{2-\delta}S$

Figure 11 shows σ_e, $\Delta(en)/\Delta\varepsilon(\varepsilon\equiv eE/kT)$, $\Delta\sigma_e/\Delta(en)$, $R\sigma_e$ and θ, all plotted against E at 100°C. θ is plotted with linear scale (the right-hand ordinate) while the others are with log scale. This temperature is attained by lowering the temperature from higher temperatures

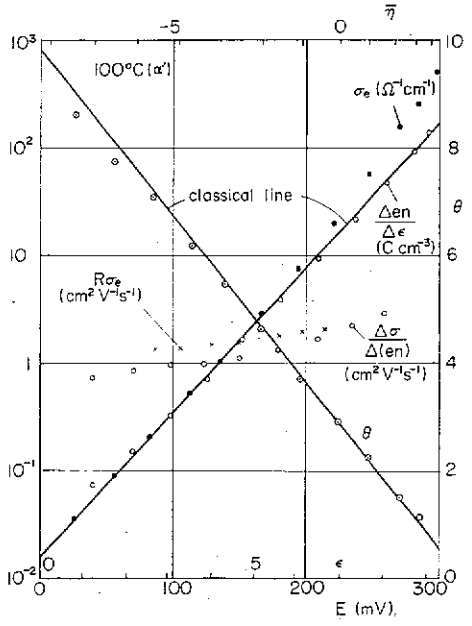

Fig. 11. σ_e, $\Delta(en)/\Delta\varepsilon$, $\Delta\sigma_e/\Delta(en)$, $R\sigma_e$ and θ vs E for α'-$Cu_{2-\delta}S$ at 100°C.

(Note the hysteresis at the transition temperature.). From the figure we see: (i) The observed values of $\Delta(en)/\Delta\varepsilon$ and of θ lie on the straight lines (indicated as "classical lines" in the figure), i.e. $\log \Delta(en)/\Delta\varepsilon = \varepsilon \times \log e - \text{const.}$ and $\theta = \text{const.} - \varepsilon$ respectively. This suggests that holes obey classical statistics and that the relations $\eta = \varepsilon + \eta_0$ and $n_d = n_h$ are well satisfied. Then we should have $\Delta(en)/\Delta\varepsilon = en$. For $E <$ 100 mV, however, there appears slight deviation from the classical lines. As the temperature is raised, the deviation becomes small and negligible at 180°C. It may be attributed to the trapping of hole at some impurities or defects. In fact it is at variance from specimen to specimen. From θ and en, we have $m^* = 2.34\, m$ under the assumption of energy independent mobility. (ii) As E increases, σ_e increases along the classical line for $E < 100$ mV, but it increases more and more rapidly. Consequently, $\Delta\sigma_e/\Delta(en)$ is not constant but increases with E. This increase may be ascribed to the trapping of hole for $E < 100$ mV, but, for $E > 100$ mV, it may be ascribed to the increase of the mobility itself with increasing E as justified by the values of $R\sigma_e$. (iii) However, there appear some difficulties. If we take $m^* = 2.3\, m$ and $\mu = 1$ cm^{2}V^{-1} s^{-1}, we have the mean free path length as small as 1 Å, showing that the ordinary band conduction model is not valid. In contrast, when E becomes large, the mobility becomes large and, in addition en becomes so large that the degeneracy becomes fairly high. For example, at 280 mV, en is 100 C cm^{-3} and μ is estimated to be 2.0 cm^{2}V^{-1}s^{-1} with the use of eq. (6). Then $\eta = 3.4$ and the mean free path length is 3.0 Å if m^* is assumed as 2.3 m as before, showing that Boltzmann equation is barely applicable. But another difficulty appears. That is, the degeneracy is expected to be fairly high, but, nevertheless $\log(en)$ vs E or θ vs E is kept along the classical line as stated above. If we assume that E does not represent the Fermi kinetic energy, then we are just in the similar situation to the case of $Cu_{2-\delta}Se$. The $\log(en)$ vs θ plot can be well fitted to the theoretical one with constant m^* and τ. In the similar way to the case of $Cu_{2-\delta}Se$, we get $m^* = 2.3\, m$ and the values of $\bar{\eta}$ corresponding to those of E as shown on the upper abscissa of Fig. 11.

(*d*) β-Cu_2S

Figure 12 shows σ_e, $\Delta(en)/\Delta\varepsilon$, $\Delta\sigma_e/\Delta(en)$ and

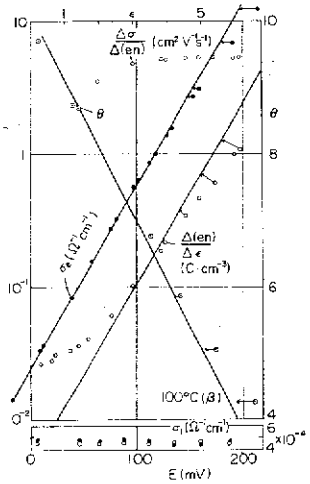

Fig. 12. σ_e, $\Delta(en)/\Delta\varepsilon$, $\Delta\sigma_e/\Delta(en)$, θ and σ_i vs E for β-$Cu_{2-\delta}S$ at 100°C.

θ vs E at 100°C. This temperature is attained by raising the temperature from the lower in contrast to the case of Fig. 11. The ionic conductivity σ_i is also shown below it; solid circles show the values obtained by the dynamic method and empty circles are from the steady state method described in §1, two methods yielding the same values. We note here (i) for $E < 140$ mV, σ_e is along the classical line, while $\Delta(en)/\Delta\varepsilon$ deviates from it more remarkably than α' phase. This deviation may be due to the trapping of holes by impurities as in α' phase, for σ_e increases rapidly with increasing temperature for small E (Fig. 6, specimen k) and the deviation differs from specimen to specimen. (ii) $\Delta\sigma_e/\Delta(en)$ decreases with decreasing E for $E < 100$ mV. This is due to the trapping of hole as stated above. For larger E, however, $\Delta\sigma_e/\Delta(en)$ becomes constant, which means the constant mobility. It seems therefore that the hole mobility is independent of E for the whole range of E. Hence, assuming constant m^* and τ, we have $m^* = 1.28\, m$ from en and θ. The mean free path is estimated as about 4 Å and the band conduction treatment may be barely applicable. (iii) For $E > 140$ mV, σ_e, $\Delta(en)/\Delta\varepsilon$ and θ deviate from the classical lines. The deviations are opposite to those in α' phase. This seems to be caused by the fact that β phase is not of average structure as seen from the rapid increase of σ_i with increasing temperature. The chemical potential of copper ions may be dependent of δ and contribute to the variation

of e.m.f. of the cell. If an appropriate correction is made to E values for σ_e-E plot as indicated by the horizontal arrows in the figure so as to make the observed σ_e values to lie on the classical line, then the observed values of $\Delta(en)/\Delta\varepsilon$ and θ are also brought on the respective classical lines as indicated.

(*e*) $Cu_{2-\delta}Se_ySe_{1-y}$

Figure 13 shows the similar plots for $Cu_{2-\delta}Se_{0.5}S_{0.5}$ at 180°C. Comparing this with Fig. 8 and Fig. 11, we see that the characteristic features of α and α' phases are not too much changed by alloying. The value of $1/R$ for α phase is larger than *en* by the factor 1.8. The difference seems larger than experimental errors but the reason of this discrepancy is unknown yet. Aside from this discrepancy, the plots shown in the figure can be well accounted for by the similar analysis made to Figs. 8 and 11, as shown by the calculated curves (broken lines) in the figure. We get $m^*=2.0\,m$ for α phase and $m^*=2.53\,m$ for α' phase. Besides, it is noticiable that the hexagonal phase is stable even below the room temperature.

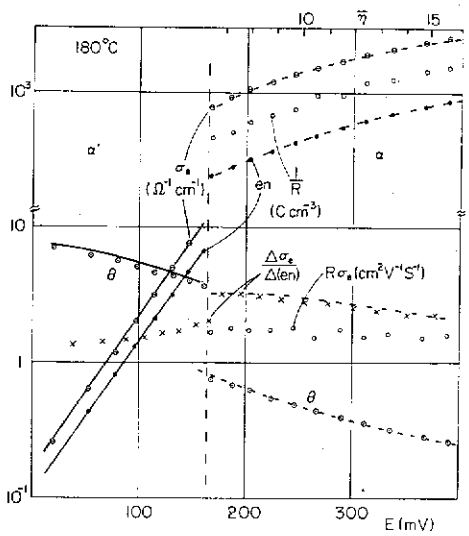

Fig. 13. σ_e, $1/R$, *en*, $R\sigma_e$, $\Delta\sigma_e/\Delta(en)$ and θ for $Cu_{2-\delta}Se_{0.5}S_{0.5}$ at 180°C.

§3. Discussion

In the preceding paragraph, we have shown that we have to use $\bar{m}^*$ and $\bar{\eta}$ in place of $\tilde{m}^*$ and ε+const. for *en* and θ to be accounted for by eqs. (2) and (4) consistently, although only *en* can be fitted to eq. (2) with $\eta=\varepsilon+$const. and $\tilde{m}^*$. From these facts we see that $\bar{\eta}$ is related to η by

$$\frac{F_{\frac{1}{2}}(\eta)}{F_{\frac{1}{2}}(\bar{\eta})}=\left(\frac{\bar{m}^*}{\tilde{m}^*}\right)^{\frac{1}{2}}\equiv\gamma, \tag{10}$$

which is reduced to $\bar{\eta}/\eta=\gamma^{-2/3}$ for large positive η and to $\bar{\eta}-\eta=-\ln\gamma$ for negative η. Figure 14 shows $\bar{\eta}$ vs ε corresponding to Fig. 8 and Fig. 11 and it also shows the calculated $\bar{\eta}$ vs η using eq. (10) with various γ-values. For Cu_2Se, $\tilde{m}^*$ is 2.9 m and $\bar{m}^*$ is 1.32 m and hence we get $\gamma=0.3$ and $\gamma^{-2/3}=2.2$ for the degenerate region. For Cu_2S, we can not be informed of $\tilde{m}^*$ value since ln (*en*) is on the classical line. But if eq. (10) is also valid for Cu_2S, the value of γ is estimated as 0.1, and it seems reasonable that ln (*en*) is on the classical line even when the degeneracy is fairly high, since $\bar{\eta}$ is large for large *en* but η is not so.

We now try to interpret eq. (10). If the position of the bottom of the valence band (see Fig. 1(b)) is lowered as *en* increases, then the increase of H becomes larger than that of eE. As the cause of such energy lowering, we may mention two factors; one is the change of lattice parameters and the other the hole-vacancy interaction. The former, however, seems to be ineffective, since *en* vs E is almost independent of Se/S ratio for the alloys Cu_2(Se, S), while the change of Se/S ratio gives rise

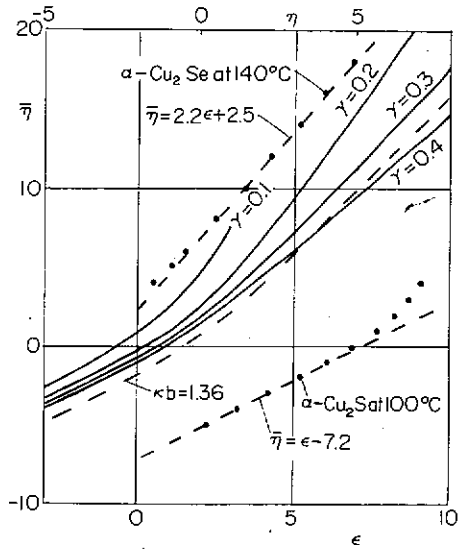

Fig. 14. $\bar{\eta}$ vs ε for α-$Cu_{2-\delta}Se$ at 140°C, $\bar{\eta}$ being indicated on the upper abscissa in Fig. 8, while ε on the lower one in the same figure, and similar plot for α'-$Cu_{2-\delta}S$ at 100°C corresponding to Fig. 11. The calculated curves are also drawn.

to a remarkable change of lattice parameters.[18] To estimate the effects of hole-vacancy interaction, we try a very simplified approach as follows.

Consider a flat potential well of radius a and depth $\hbar^2 d^2/2m^*$ and let the energy of the lowest s-state satisfying the boundary condition $\partial\psi/\partial r=0$ at $r=b$ be $-\hbar^2\kappa^2/2m^*$, where ψ is the wavefunction and b is the radius of the Wigner-Seitz like cell belonging to one vacancy, that is, $b=(3/4\pi n)^{1/3}$. We can easily get κb as a function of κa and $\sqrt{d^2-\kappa^2}a=\omega a$. If $\omega a\simeq\pi/2$ (The discrete level appears at $b\to\infty$ for $\omega a>\pi/2$), κb becomes nearly independent of the ratio b/a. For example, $\kappa b=1.36\sim1.40$ for $3.5<b/a<10$ if $\omega a=1.6$. Thus we may take κb as a constant which is independent of the carrier concentration, if we assume a properly deep potential well. Since the lowest energy corresponds to the bottom of the band, the lowering $\Delta\eta$ which is reduced to non-dimensional is given by $\Delta\eta=\hbar^2(\kappa b)^2/2m^*kTb^2$, where we assume the effective mass is not affected by energy lowering. With $b=(3/4\pi n)^{1/3}$, it is reduced to

$$\Delta\eta=(\kappa b)^2\left(\frac{4}{9\pi}\right)^{\frac{2}{3}}\left(\frac{3}{2}F_{\frac{1}{2}}(\bar{\eta})\right)^{\frac{2}{3}}. \qquad (11)$$

Putting $\Delta\eta=\bar{\eta}-\eta$, we have η as function of $\bar{\eta}$, which is to be compared with ε vs $\bar{\eta}$ apart from an additive constant for ε. The broken line in Fig. 14 is the calculated one with $\kappa b=1.36$, accounting for the experimental plots for Cu_2Se. The depth of potential is $1.6^2\times\hbar^2/2m^*a^2$ if we neglect $(\kappa a)^2$ against $(da)^2$. Since a is expected to be a few Å, the well is very deep.

We may also interpret this energy lowering by the following way. Let us assume that a certain fraction of holes s is gathered in a small volume v around each vacancy and the other holes are distributed with the effective mass m^* in the remaining space nearly free from the vacancy field. Then we have

$$\frac{(m^*/m)^{\frac{3}{2}}N\frac{3}{2}F_{\frac{1}{2}}(\eta)}{n}=\frac{1-s}{1-nv}\equiv\bar{S}. \qquad (12)$$

If we assume $\bar{S}$ as constant, eq. (12) becomes consistent with eq. (10), leading to $m^*/\bar{m}^*=\bar{S}^{2/3}$. Then, we have $\gamma=(\bar{m}^*/m^*)^{3/2}\bar{S}$. On defining $\bar{m}^*$, we assume that there is no substantial difference between the shielding holes and remaining holes as far as the transport properties are concerned. Therefore, $\bar{m}^*$ may be equal to m^*. This will well hold especially for the degenerate case since only the holes near the Fermi level are concerned in this case. If we further neglect nv compared to unity in $\bar{S}$, we have the simple relation as $\gamma=1-s$. For example, the vacancy in Cu_2Se is shielded by 0.7 of holes.

At the present stage, the above discussions have only phenomenological meaning. We hope more detailed discussions and experimental justifications will be done in future.

Acknowledgements

The authors wish to express their hearty thanks to Professor T. Shimizu and Dr. M. Kimura for their valuable discussions and encouragements.

References

1) P. Rahlfs: Z. phys. Chem. B **31** (1936) 157.
2) E. H. Roseboom, Jr.: Econ. Geol. **61** (1966) 641.
3) S. Djurle: Acta. Chem. Scand. **12** (1958) 1427.
4) R. D. Heyding: Canad. J. Chem. **44** (1966) 1233.
5) P. Kubaschewski and J. Nölting: Ber. Bunsenges. physik. Chem. **77** (1973) 70.
6) P. Kubaschewski and J. Nölting: Ber. Bunsenges. physik. Chem. **77** (1973) 74.
7) V. H. Konev and V. A. Kudinova: Inorg. Mater. (USA) **9** (1973) 1008. translation: Izv. Akad. Nauk SSSR Neorg. Mater. **9** (1973) 1132.
8) M. Reinhold and H. Möhrung: Z. phys. Chem. B **38** (1938) 221.
9) E. Hirahara: J. Phys. Soc. Japan **6** (1951) 422
10) S. Miyatani and Y. Suzuki: J. Phys. Soc. Japan **8** (1953) 680.
11) K. Okamoto: Japan. J. appl. Phys. **8** (1969) 718.
12) K. Okamoto and S. Kawai: Japan. J. appl. Phys. **12** (1973) 1130.
13) J. B. Wagner and C. Wagner: J. chem. Phys. **26** (1957) 1602.
14) *For example*, J. Mahenc, R. Routie and P. Taxil: J. chem. Phys. **67** (1970) 73.
15) T. Takahashi and O. Yamamoto and S. Ikeda: J. Electrochem. Soc. Solid-State Science and Technology **120** (1973) 1431.
16) I. Yokota: J. Phys. Soc. Japan **16** (1961) 2213.
17) S. Miyatani: J. Phys. Soc. Japan **14** (1959) 996.
18) Y. G. Asadov, G. A. Jabrailova: Kristall und Technik **8** (1973) 449.